Lithos 148 (2012) 98–111

Contents lists available at SciVerse ScienceDirect

Lithos

journal homepage: www.elsevier.com/locate/lithos

Post-collisional transition from an extensional volcano-sedimentary basin to a continental arc in the Alborz Ranges, N-Iran

Abbas Asiabanha [a,*], John Foden [b]

[a] Department of Geology, Faculty of Science, Imam Khomeini International University, Qazvin, Iran
[b] School of Earth and Environmental Sciences, Adelaide University, Adelaide, SA 5005, Australia

ARTICLE INFO

Article history:
Received 20 September 2011
Accepted 17 May 2012
Available online 26 May 2012

Keywords:
Back-arc
Subduction
Neotethys
AFC modeling
Alborz
Iran

ABSTRACT

The Alborz Magmatic Assemblage (AMA) is an Eocene volcanic complex in northern Iran, and is situated at the site of the closure of the Tethyan basin. The magmatic rocks of the Alborz assemblage exhibit a distinct progression in style, from shallow submarine explosive eruptions to more effusive sub-aerial eruptions. Their chemical compositions indicate that they belong to the high-K calc-alkaline (shoshonitic) suite, and are related to either a subduction regime or continental collision. This conclusion is verified by major and trace element abundances, such as enrichments in Light Rare Earth Elements (LREEs) and Large Ion Lithophile Elements (LILEs) (e.g., K, U, and Sr) and depletion in High Field Strength Elements (HFSEs) (e.g., Nb, Ta, Ti, and Zr). However, HFSE plots suggest that the source region of the AMA magmas was affected by multiple processes, including deeply subducted lithosphere and the partial melts of extensional lithosphere in a back-arc environment.

The isotopic composition of this suite and their trace element ratios suggest that the primary magmas were derived from a depleted mantle source and were subsequently affected by both fractional crystallization (ol + cpx in basic magmas and plg + bio ± hbl in intermediate magmas) and assimilation during magmatic evolution. Assimilation and fractional crystallization modeling, based on isotopic and trace element ratios, indicates that the ascending magmas were contaminated by approximately 40% continental crust.

The petrography and geochemical composition of the Eocene Alborz magmatic assemblage indicate that it developed in a back-arc basin, in which explosive eruptions produced various pyroclastic and epiclastic deposits. A subsequent stage of volcanism then produced more effusive sub-aerial eruptions, as well as sporadic explosions that generated ignimbritic sheets.

1. Introduction

The Alborz Range of Northern Iran (approximately 600 km long and 100 km wide) is a part of the largest mountain belt of the world—the Alpine–Himalayan Belt—and is situated between the Caspian Sea to the north and the Iranian Plateau to the south. It extends westwards into the Pontides Arc (Turkey) and the Lesser Caucasus (Armenia) (Fig. 1). The range has many summits with elevations of 3600–4800 m, culminating in the Quaternary volcano of Damavand (5671 m) in the center of the belt (Jackson et al., 2002).

The Alborz Range is the result of multiple tectonic events, extending from the late Triassic Cimmerian Orogeny, which resulted from collision of the Iranian block with the Eurasian plate, to present-day on-going intra-continental deformation related to continued convergence of the Arabian and Eurasian plates.

Cenozoic magmatic rocks are found throughout the peri-Arabian region, to the north of the Zagros–Bitlis suture zone. Although they range in age from Eocene to Quaternary, their temporal distribution is focused into several pulses of magmatism in the Eocene, Miocene, and Plio-Quaternary. The most significant volcanic provinces in Iran are divided into three zones: the Urumieh–Dokhtar Magmatic Assemblage (UDMA), the Alborz Magmatic Assemblage (AMA; Fig. 1), and the East Iran Magmatic Assemblage (EIMA). The two former zones have a general trend parallel to the Neotethyan suture zone (or Zagros suture zone), and display geological and geochemical characteristics that relate them to the Neotethyan ocean (e.g., Alavi, 2004, 2007; Allen et al., 2003; Asiabanha et al., 2009; Axen et al., 2001; Berberian and King, 1981; Berberian et al., 1982; Dargahi et al., 2010; Ghasemi and Talbot, 2006; Shahabpour, 2005; Zanchi et al., 2006). Although many studies have investigated the relationship between volcanism and subduction/collision in the UDMA, less is known of the AMA.

It seems likely that the Zagros–Bitlis suture is indeed the closed remnant of Tethys and that the UDMA and AMA magmatic belts formed on the upper plate, underthrust by Tethyan subduction towards the north/

* Corresponding author. Tel./fax: +98 2813780040.
E-mail addresses: asiabanha@ikiu.ac.ir (A. Asiabanha), john.foden@adelaide.edu.au (J. Foden).

0024-4937/$ – see front matter © 2012 Elsevier B.V. All rights reserved.
doi:10.1016/j.lithos.2012.05.014

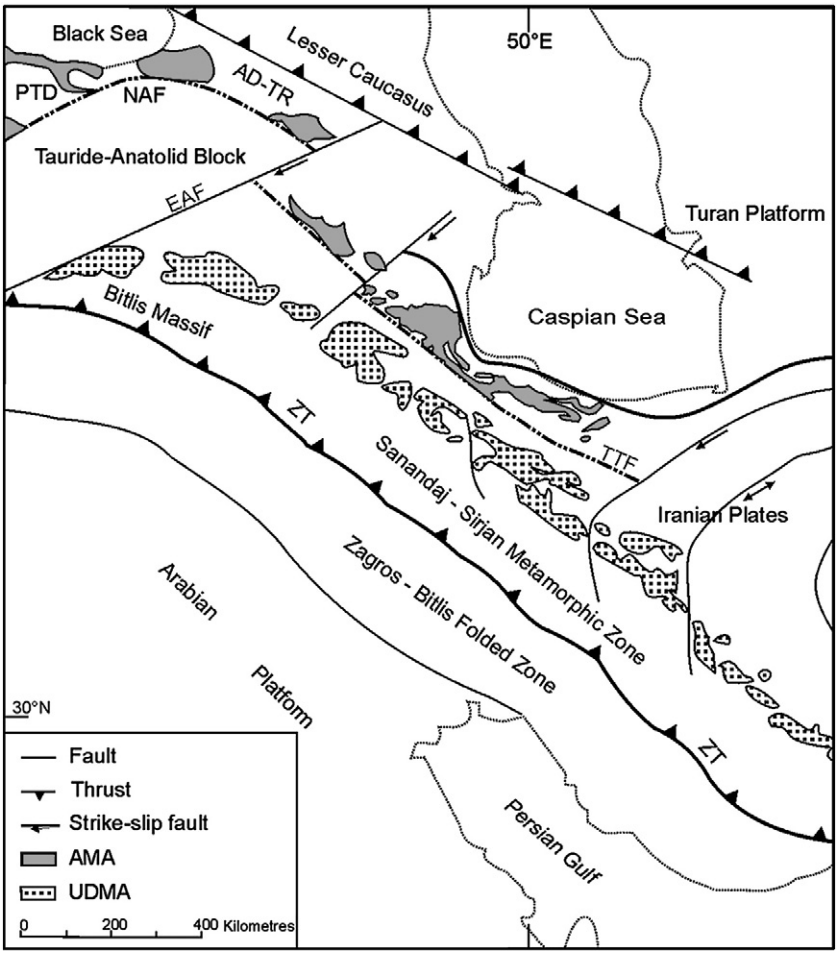

Fig. 1. Simplified tectonic map of the Iranian–Turkish Plateau (modified and simplified after Alavi, 2007; Brunet et al., 2003; Vincent et al., 2005). Abbreviations are as follows: AD-TR = Adjaro-Trialet; AMA = Alborz Magmatic Assemblage; EAF = East Anatolian Fault; NAF = North Anatolian Fault; PTD = Pontides; TTF = Tabriz–Takestan Fault; UDMA = Urumieh Dokhtar Magmatic Assemblage; ZT = Zagros Thrust.

north east (Omrani et al., 2008). In this case, the AMA belt is more distal to the Cretaceous to Eocene trench (200–500 km) relative to the UDMA belt. This may suggest that the more long-lived UDMA belt is the main magmatic arc, while the AMA is perhaps formed in an extensional, back-arc regime. Definitive petrological studies of the AMA suites have not until now been made, and this has restricted comparisons between the UDMA and the AMA belt.

Previous studies that examined the Turkish Plateau (e.g., Sosson et al., 2010 and references therein) have shown that the Neotethyan ocean had distinct northern and southern branches. The northern branch lay between the Pontides and the Taurides–Anatolide–South Armenia (TASA) blocks, whereas the southern branch was situated between the TASA block and the Afro-Arabian plate (Fig. 1). The two suture zones converge at the northwestern border of Iran, and grade into the Tabriz Thrust (northern branch) and Zagros Thrust (southern branch).

The continuation of the Zagros Thrust as the Neotethyan suture zone is agreed upon by most authors (e.g., Agard et al., 2005; Berberian and King, 1981; Ghasemi and Talbot, 2006; McCall, 1997; Stampfli, 2000; Stöcklin, 1974; Vincent et al., 2007), whereas the Tabriz–Takestan Fault is not considered part of the suture zone. However, Alavi (1996, 2007) proposed that the Tabriz–Takestan Fault may be a Neotethyan continent–arc collision suture, and in recent years other authors have suggested that a back-arc basin was closed along the Tabriz–Takestan Fault (e.g., Azizi and Moinevaziri, 2009).

Accordingly, the main objectives of this contribution are to systematically investigate the different eruption styles of the AMA, as well as its main petrogenetic and tectono-magmatic features. In this study, we have employed facies analysis, in combination with measurements of major, trace element and isotope compositions, to investigate Neotethyan-related magmatism in the AMA, as well as the occurrence of other synchronous magmatic arcs (e.g., the UDMA).

2. Regional geology

The Alborz Mountains consist of old basement (Late Precambrian) with a Gondwanan affinity, similar to the Arabian–Nubian platform (e.g., Hassanzadeh et al., 2002). During the Paleozoic it was part of Gondwana at the southern margin of the Paleotethys Ocean. It then separated from Gondwana at 290 Ma, forming the Neotethys Ocean before the Alborz collided with Eurasia at 235 Ma (Berberian, 1981; Stampfli, 2000; Stampfli et al., 1991; Stöcklin, 1974).

The Late Cretaceous is represented by several facies in the Alborz, such as volcanics and volcano-sediments in the western Alborz, and a thick series of carbonates and marls in north–central Alborz. Compressional deformation may have occurred during pre-Eocene times (Brunet et al., 2003).

The Cretaceous to Eocene succession represented a transition from a period of tectonic quiescence during the Jurassic and Cretaceous, to a period of regional compression from the end of the Cretaceous to the Paleocene (Berberian and King, 1981; Stöcklin, 1974). However, Wensink and Varekamp (1980) showed that basaltic volcanism in the central Alborz commenced in the Neocomian (Barremian alkaline

olivine basalts) and continued into the Turonian and Lower Senonian (high-alumina basalts).

The Eocene was a time of extensive volcanic eruptions in Iran, especially in the Alborz and Urumieh–Dokhtar zones. The products of these eruptions (the Karaj Formation) were deposited in central and western Alborz within an extensional regime (Allen et al., 2003; Ballato et al., 2010; Berberian, 1983; Hassanzadeh et al., 2002).

During the Oligocene and Miocene, the region experienced uplift caused by the collision of Arabia with the Iranian terranes; at the same time, continental sediments were deposited in intermountain basins (red beds). The Cenozoic succession within and adjacent to the Alborz coarsens upwards, suggesting an increase in the subaerial relief of the range with time. This is consistent with active compressional deformation from the Pliocene to the Quaternary, for which there is abundant evidence (Alavi, 1996; Brunet et al., 2003; Stöcklin, 1974).

3. Karaj Formation in the AMA: facies and petrography

The Eocene volcaniclastic and volcanic sequence of the Karaj Formation has a maximum thickness of 5 km, and is exposed mainly in the southern Alborz. The succession is composed of clastic sedimentary and volcaniclastic deposits in the lower parts, and potassic calc-alkaline basic to acidic lava flows in the upper parts. Large-scale slumps (Lasemi, 1992), microfauna (e.g., Asiabanha et al., 2009), and organic-rich mudstones in the middle of the succession (Allen et al., 2003) may indicate a relatively deep-water trough. This interpretation is consistent with the occurrence of thick (>5 km) Paleocene–Eocene turbidites (Allen et al., 2003), decreasing to a thickness of 3 km in the east (Brunet et al., 2003). The thickness of flows and the ratio of lava to volcaniclastics show an increase westwards. Because of rapid changes in the thickness, composition, and color of pyroclastic deposits in the AMA, various classification schemes were employed by pioneering geologists in the 1960s and 1970s (Annells et al., 1975; Dedual, 1967; Stöcklin and Eftekhar-Nezhad, 1969). However, as noted by Annells et al. (1975), these classifications have a local rather than regional significance. Accordingly, these volcaniclastic and volcanic deposits are more effectively classified using facies analysis and eruption style, rather than by application of lithological characteristics alone (Asiabanha, 2006).

3.1. Volcaniclastic deposits

Volcaniclastic deposits in the Alborz Ranges are mainly found in central Alborz, and were primarily described by Dedual (1967) as the "Karaj Formation". Based on stratigraphic relations and fossils, he placed the formation within the Eocene, and divided its 3300 m succession into five units (from oldest to youngest): Lower Shale, Middle Tuff, Asara Shale, Upper Tuff, and Kandovan Shale. These units were recently dated using the U–Pb method by Verdel (2008), with the following results: Middle Tuff = 49.3 ± 2.9 Ma, Asara Shale = 45.3 ± 2.3 Ma, and Upper Tuff = 41.1 ± 1.6 Ma. In addition, radiometric dating of the Karaj Formation by Ballato et al. (2010) using different minerals (zircon and biotite) indicates that this volcano-sedimentary event occurred between 47.4 ± 3.8 and 36.0 ± 0.2 Ma. Thus, the authors estimated that volcaniclastic deposition in the central Alborz Mountains lasted for at least 11.4 ± 0.4 Ma.

The occurrence of evaporative gypsum lenses in the uppermost parts of volcaniclastic deposits throughout the Alborz (e.g., Gachsar and Alamout), combined with intense folding of tuffs in the Alamout (Qazvin) and Jirandeh (Lushan), shows that the volcano-sedimentary trough was uplifted by compressive stresses in the late Eocene and eroded. Moreover, the Karaj Formation is unconformably overlain by upper Eocene evaporites of the Kond Formation, indicating that the volcano-sedimentary basin was uplifted within a compressional regime in the late Eocene.

3.2. Lava flows

Although Eocene volcanism in the central Alborz is dominated by pyroclastic deposits (green tuff and lapilli tuff), lava flows of a different composition cover the underlying pyroclastic deposits in the western Alborz. The common occurrence of red soil horizons under the basic flows, together with columnar jointing, suggests that they are the products of sub-aerial eruptions. The most important petrographic features and characteristics of the lava flows in the AMA are as follows:

1) *Basalt–Trachybasalt* contains phenocrysts of plagioclase (An_{55-65}) + olivine + augite + Fe–Ti oxide ± biotite ± hornblende ± apatite, and has a hyalo- to microlitic porphyritic texture. Plagioclase typically exhibits zoning (oscillatory and reverse), reaction rims, and sieve textures.
2) *Andesite–Trachyandesite* contains phenocrysts of plagioclase (An_{36-61}) + sanidine + hornblende ± biotite ± augite ± olivine ± quartz + Fe–Ti oxide + apatite, set in a pilotaxitic or trachytic groundmass.
3) *Dacite–Rhyolite* contains plagioclase (An_{45-50}) + sanidine + quartz + phlogopite ± hornblende ± apatite with minor augite and Fe–Ti oxides, and has a porphyroclastic, eutaxitic (ignimbrite), or microporphyritic (dome) texture.

3.3. Sub-volcanic (intrusive) bodies

Intrusive bodies in the AMA are typically small (dikes, stocks, and laccoliths) and have the same composition as volcanic rocks. However, basic–intermediate rocks, including monzodiorite, monzogabbro, monzonite, and syenite, are more abundant than felsic varieties. The following descriptions are of typical members of the AMA intrusive suite.

(1) A monzonitic laccolith (>30 km^2 in area) contains K-feldspar (~30%), plagioclase (~25%–30%), clinopyroxene (~10%–15%), olivine (<2%), and biotite (<5%), along with minor orthopyroxene, apatite, and opaques.
(2) Gabbroic dikes contain plagioclase (~35%–40%), augite (~35%), olivine (~5%–10%), biotite (<3%), apatite (~2%), and opaques (~10%), and have a granular or ophitic texture.
(3) Syenitic dikes contain subhedral to anhedral microperthite (~85%–90%), plagioclase (<5%), quartz (<5%), and minor opaque minerals, apatite, and biotite.
(4) A monzogabbroic stock (~1 km^2 in area) contains medium-grained plagioclase (~35%), augite (~30%), and olivine (~5%), with minor biotite, apatite, and opaque minerals.
(5) A monzogranitic stock (~1–3 km^2 in area) is grey to pink in color and has a microgranular to hypidiomorphic granular texture (locally granophyric and porphyritic granular), containing quartz (~28%), plagioclase (~35%–40%), K-feldspar (~22%), and minor biotite, muscovite, and apatite.

4. Geochemistry

During systematic investigations of the western AMA, more than 60 samples were taken from different localities within this volcano-plutonic complex. Samples were crushed, pulverized in an agate mill, and analyzed by inductively coupled plasma-mass spectrometry (ICP-MS) at Actlabs (Canada) using the lithium metaborate/tetraborate fusion ICP Whole Rock Package. A portion of sample pulp was mixed with flux (lithium metaborate, $LiBO_2$) to lower its melting point. The mixture was then heated in a muffle furnace until molten. After cooling, the fused mass was digested in 5% HNO_3 and the resulting clear solution was analyzed.

In addition, a subset of samples was analyzed by X-Ray Fluorescence (XRF) at the Geological Society of Iran (GSI), Tehran, Iran. Also included

Table 1
Representative major (wt.%) and trace element (ppm) compositions of volcanic rocks from the Alborz magmatic assemblage, northern Iran.

Sample	AL-1	AM-4	AM-10	Zar-2	SZ-3	B-10	K37	B.01	B14-9	BA-1	BA-19	A.1	A.13	A.Ch.1	M24	M50	M16	SOL-1	A-131	As.S.1	M.2
Rock type	Trachybasalt–trachyandesite														Dacitic domes				Dacitic ignimbrites		
SiO_2	63.30	51.09	50.57	54.43	59.39	56.70	58.77	49.13	52.50	47.10	55.30	56.11	58.43	49.36	67.58	64.63	64.61	68.65	65.26	64.21	65.63
TiO_2	0.6	0.81	0.83	0.95	0.72	0.75	1.22	0.95	1.23	1.84	0.89	0.87	0.93	1.08	0.55	0.78	0.79	0.26	1.12	0.57	0.44
Al_2O_3	17.76	17.35	16.76	18.6	16.4	17.25	15.60	16.76	16.85	16.3	14.75	16	17.45	16.99	14.63	15.22	15.20	17.3	16.52	16.19	16.16
Fe_2O_3	5.07	7.79	8.14	7.36	6.37	7.08	7.78	10.13	9.34	11.25	6.9	7.15	7.78	9.73	3.58	3.93	4.19	2.39	3.89	4.01	3.89
MnO	0.08	0.13	0.07	0.09	0.05	0.09	0.15	0.16	0.13	0.11	0.13	0.13	0.05	0.13	0.10	0.06	0.10	0.07	0.08	0.06	0.07
MgO	2.09	5.66	6.06	2.47	2.51	2.51	1.81	7.48	4.66	4.84	4.34	2.87	1.26	5.52	1.05	1.33	2.13	0.87	2.99	1.65	0.86
CaO	3.43	9.15	8.58	7.57	4.81	4.88	5.39	10.92	6.23	9.35	6.43	7.02	4.99	9.93	1.52	2.24	1.90	2.59	4.27	3.54	3.33
Na_2O	4.53	2.96	3.43	3.21	3.22	3.4	3.24	2.22	4.19	3.43	2.93	3.72	3.54	2.82	5.43	5.03	4.58	4.27	2.96	3.49	3.23
K_2O	2.86	3.06	3.43	2.79	4.39	2.55	4.13	1.97	2.47	1.56	3.45	3.24	3.73	1.86	2.48	2.61	2.93	3.45	2.57	3.82	4.41
P_2O_5	0.3	0.13	0.17	0.27	0.15	0.27	0.41	0.32	0.52	0.28	0.31	0.27	0.3	0.31	0.10	0.14	0.21	0.17	0.21	0.16	0.18
LOI						4			2.44	4.42	5.01	2.3	1.23	1.97						1.98	1.45
Total	100.03	98.13	98.45	97.74	98.01	99.8	98.50	100.04	100.5	100.5	100.5	99.68	99.69	99.7	97.02	95.97	96.64	100.02	99.87	99.68	99.65
V	54	137	161	195	150	132	170	247	191	279	154	183	187	265	60	45	45	13	68	80	90
Cr	<20	48.2	53.2	40	50	30	30	80	50	200	170	57.3	60.3	55.3	20	10	10	<20	74	15.8	9.9
Co	7	37.33	28.87	17.5	19	14.9	18.5	30	26.4	45.8	22	20.1	17.4	30.5	5	3	5	2	7	9	9.6
Ni	<20	51	15.2	15	35	<5	15	50	19	119	34	21.4	21.1	35.2	5	5	5	<20		6.9	6.3
Zn	60	262	720	85	80	95	105	70	87	105	102				155	105	95	60	91		
Ga	15	10	21	20	17	19.9	20	12	21.4	17	18.7				16	18	19	15	20		
Rb	77	110	108	73.2	135.5	51.5	121	43	94.2	28.5	103.5	104	134	35	70.6	46.5	61.6	102	137	116	133
Sr	284	746	676	550	424	1080	401	460	694	571	516	366	422	535	160.5	117	144.5	329	298	303	462
Y	24.4	19.6	12.8	27	22	19.7	41	19.7	23	22	23.2	22.16	19.74	19.16	27	36.5	36	18.9	4.3	22.91	12.71
Zr	166	302	285	155.5	184.5	168	254	89	180	148	191	222	237	92	202	172	178	219	147	254	163
Nb	14	15	14	13	16	12.8	21	6.7	21.3	36.3	15.6	16.1	15.9	7.7	18	13	14	12.7	2.4	16.1	12.4
Sn	2	191	190	2	2	2	3	1	5	5	3				3	2	2	2			
Cs	0.8	8.71	8.84	0.9	3.7	0.26	2.9	1.1	2.23	0.8	3.16				0.5	0.9	0.7	2.9	7.3		
Ba	729	575	398	595	577	1440	810	451	586	590	692	640	704	527	557	665	499	858	656	863	912
La	33.8	29.25	29.7	29	29.5	32.7	45.5	18	41.3	28.9	36.4	22.46	24.95	16.24	35	31	32	34.8	33.68	30.34	28
Ce	64.2	64.5	63.9	54.5	52	62.6	87.5	36.8	78.3	54.8	71.1	51.21	57.38	30.35	64	63	64	64.5	49.2	60.88	53.6
Pr	7.1			6.7	6.4	7.33	10.8	4.5	9.38	6.37	8.39	5.74	6.36	3.89	7.3	7.9	8	6.77		7.11	5.6
Nd	26.1	40	24	26.5	22.5	26.8	41.5	18.9	35.3	24.2	30.3	22.67	25.1	17.24	26	31	32	23.3	32	24.82	19.82
Sm	5.12	0.44	2.89	5.5	4.6	5.07	8.5	4.4	7.12	4.87	6.22	4.44	4.7	3.79	4.8	6.5	6.8	4.15	1.97	4.58	3.33
Eu	1.33	1.1	1.39	1.5	1.2	1.46	1.9	1.4	2.11	1.89	1.49	1.14	1.16	1.2	1.2	1.8	1.8	1.05	1.04	1.06	0.91
Gd	4.56	1.6	1.5	5.5	4.7	4.93	8.8	4.5	6.56	5.5	5.76	4.13	4.2	3.86	4.9	7	6.8	3.52	1	4.12	2.7
Tb	0.71	0.44	0.79	0.8	0.7	0.71	1.2	0.7	0.92	0.78	0.83	0.6	0.63	0.62	0.7	1.1	1.1	0.55	0.49	0.55	0.38
Dy	4.13	3.76	3.28	4.6	3.7	3.96	7.2	4.0	4.85	4.48	4.56	3.98	3.73	3.5	4.4	6.4	6.4	3.29	2.12	3.66	2.32
Ho	0.78	0.44	0.4	1	0.8	0.81	1.4	0.8	0.96	0.91	0.94	0.75	0.69	0.7	0.9	1.3	1.3	0.64	0.62	0.75	0.42
Er	2.35			2.9	2.4	2.27	4.3	2.2	2.56	2.48	2.63	2.17	2.11	1.98	3	4.1	4.1	2		2.16	1.37
Tm	0.37	0.43	0.18			0.35	0.6	0.3	0.37	0.31	0.4	0.33	0.35	0.29	0.5	0.6	0.6	0.33	0.31	0.36	0.22
Yb	2.43	2.65	3.22	2.7	2.4	2.08	3.8	1.9	2.18	2.14	2.39	2.13	2.08	1.83	3	3.9	3.8	2.27	1.33	2.25	1.33
Lu	0.37	0.53	0.46	0.4	0.4	0.34	0.6	0.3	0.33	0.34	0.38	0.36	0.35	0.29	0.5	0.6	0.6	0.34	0.303	0.38	0.24
Hf	4.4	8.6	6.1	5	6	4.5	7.0	2.2	4.5	3.8	5.2	5.8	6.3	3	6	5	6	5.2	5.44	7.1	4.6
Ta	1.14	0.75	0.54	0.5	1	1	1.5	0.4	1.5	2.5	1.3	5.8	1.2	0.4	1	0.5	0.5	1.06	0.44	0.4	0.2
W	1.7	94.5	40.3	3	4	4	4.0	0.7	4	5	5				3	3	3	2.5	11.46		
Th	11.7	14.44	14.04	7	12	10.1	12.0	2.4	9.06	3.6	15.05	12.5	15.1	8.1	12	7	7	10.2	8.62	11.2	8.4
U	3.81	13.50	15.04	1.50	3.50	2.68	3.00	0.71	2.32	0.60	4.25	3.5	3.2	0.9	3.00	2.00	1.50	3.18	9.88	3.9	2.2

Table 2
Representative major (wt.%) and trace element (ppm) data for plutonic (sub-volcanic) rocks from the Alborz magmatic assemblage, northern Iran.

Sample	B9	BA-9-1	BA-11-1	BA-13-2a	GAR-2	G.02	M14	S12	B14-6	S4	M11*	S3*	BA-13-1b*
Rock type	G	G	G	G	G	MG	MG	MG	MD	S	G	G	G
SiO_2	48.30	49.80	50.10	50.70	52.80	51.92	49.21	51.96	57.80	62.35	45.42	45.86	48.00
TiO_2	0.8	1.19	1.18	1.34	0.97	1.043	1.11	1.24	0.89	0.53	1.79	1.64	0.96
Al_2O_3	15.4	17	16.95	17.6	17.56	18.29	18.76	19.13	17.35	16.74	11.81	11.77	12.15
Fe_2O_3	10.05	9.35	9.84	10.8	8.25	8.89	8.8	7.35	7.19	4.13	16.26	15.75	10.1
MnO	0.17	0.15	0.17	0.18	0.19	0.165	0.16	0.12	0.12	0.08	0.24	0.23	0.16
MgO	8.09	5.44	5.94	4.95	4.29	4.8	3.38	2.1	3.2	0.81	10.1	9.94	13.65
CaO	10.55	10.35	9.56	9.36	11.23	8.38	8.43	6.24	6.08	1.33	10.47	10.36	9.83
Na_2O	2.01	2.58	2.91	3.06	2.85	2.93	3.46	4.52	3.61	3.97	1.94	1.69	1.7
K_2O	1.68	0.97	1.32	1.52	1.62	3.2	2.69	3.52	3.26	7.83	1.44	1.33	1.24
P_2O_5	0.24	0.18	0.24	0.24	0.28	0.41	0.38	0.39	0.37	0.06	0.43	0.26	0.19
LOI	2.4	3.54	1.27	0.29					0.49				2.15
Total	99.8	100.5	99.6	100	100.04	100.028	96.38	96.57	100.5	97.83	99.9	98.83	100.5
V	242	245	200	262	210	222	215	140	141	10	535	391	192
Cr	320	160	90	90	160	50	50	30	120	20	190	204	1100
Co	41.7	31.6	32.8	33.5	24	22	24.5	14	18.7	4	59.5	59.5	53.3
Ni	63	23	18	10	60	40	35	10	23	5	100	117	299
Zn	82	114	93	105	70	80	105	80	101	90	135	125	84
Ga	15	18.8	19.8	21.6	14	14	20	22	20.9	22	17	15	13.8
Rb	38.5	22.6	26.7	32.5	32	83	69.6	84.2	100.5	172	34.6	29.6	31.8
Sr	507	484	462	595	492	553	741	715	633	188	418	435	445
Y	13.2	17.7	21.7	23.6	22.6	23.6	25	31.5	21.4	41	22.5	19.8	14.7
Zr	58	93	146	169	110	142	119.5	154	218	480	78	71.4	57
Nb	5.5	7.8	12.4	13.4	8.8	12.3	11	17	18.8	33	7	7	5.1
Sn	1	2	2	2	2	2	1	1	3	4	1	1	2
Cs	0.93	0.5	0.48	0.62	0.7	3.5	1.1	14.1	3.58	1	1.5	1.4	1.4
Ba	265	298	462	440	572	631	543	909	732	641	354	340	248
La	11.2	16.8	26	28.7	24.6	27.8	29	38	39.4	59.5	18.5	15.4	10.3
Ce	22.2	33.6	52.7	57.5	49.9	55.1	55.5	69.5	75.2	108	35	32.8	22.8
Pr	2.9	4.26	6.49	6.95	5.91	6.51	6.9	8.7	8.68	12.4	4.5	4.23	3.09
Nd	11.9	16.8	25.4	26.6	24	26.3	27.5	33.5	31	43.5	19.5	18.8	13
Sm	2.82	3.75	5.52	5.62	5.23	5.58	5.8	6.9	5.98	8.5	4.7	4.5	3.03
Eu	1	1.31	1.7	1.67	1.53	1.61	1.8	2.4	1.6	1.7	1.5	1.62	1.06
Gd	2.74	3.81	5.07	5.54	4.95	5.33	5.5	7.8	5.47	8.7	5.1	4.86	3.1
Tb	0.46	0.62	0.78	0.86	0.79	0.81	0.8	1.1	0.8	1.2	0.7	0.78	0.49
Dy	2.64	3.51	4.42	4.78	4.42	4.45	4.6	6	4.14	7.2	4.4	3.75	2.96
Ho	0.56	0.75	0.87	1	0.86	0.86	0.9	1.2	0.86	1.5	0.8	0.81	0.62
Er	1.57	2.03	2.49	2.69	2.51	2.5	2.6	3.5	2.42	4.7	2.4	2.19	1.69
Tm	0.23	0.31	0.36	0.41	0.37	0.371	0.4	0.5	0.36	0.8	0.3	0.29	0.26
Yb	1.43	1.84	2.15	2.33	2.32	2.32	2.3	3	2.11	5	2	2	1.48
Lu	0.22	0.3	0.34	0.38	0.34	0.345	0.4	0.4	0.34	0.8	0.3	0.28	0.24
Hf	1.6	2.6	3.7	4.3	3.2	3.6	3	4	5.6	13	3	2	1.7
Ta	0.3	0.7	0.9	0.9	0.56	0.78	0.5	0.5	1.6	2	0.4	0.4	0.4
W	2	2	1	5	1	2.9	4	3	3	4	3	6	1
Th	1.63	3.63	4.19	4.86	5.94	5.61	5	6	14	17	3	2.2	1.54
U	0.58	1.01	1.14	1.28	1.53	1.61	1.50	1.50	3.73	4.00	0.50	0.63	0.47

Abbreviations: G = Gabbro; MG = Monzogabbro; MD = Monzodiorite; S = Syenite. Samples numbered M11*, S3*, and BA-13-1b* are considered to be cumulates.

were 7 samples from Ebrahimi's (2000) study of the Molla-Ali district, which were analyzed by ICP-MS at the China University of Geosciences, Beijing, China (Tables 1 and 2).

Ten representative samples of the various rock units were selected for analysis of Sr, Nd, and Sm isotope ratios at the School of Earth and Environmental Sciences, the University of Adelaide, Australia. They were measured by thermal ionization mass spectrometry (TIMS) on a Finnigan MAT 262 system in static mode for Sm, and dynamic mode for Sr and Nd, using the analytical techniques described in Foden et al. (1995).

The reproducibility of the method (1 standard deviation; S.D.) is 43 ppm for $^{87}Sr/^{86}Sr$ and 58 ppm for $^{143}Nd/^{144}Nd$. Machine performance was monitored by repeat analyses of international standards. The average for SRM 987 was 0.710265 (1 S.D. = 0.000015; n = 7); for JNdi-1 it was 0.512078 (1 S.D. = 0.000008; n = 6). Whole procedure blanks were better than 1 ng for Sr and better than 200 pg for Nd.

4.1. Major element chemistry

The analyses reveal that rocks from the western AMA belong mainly to three groups: (1) shoshonite–latite (SiO_2 = 46–60 wt.%), (2) dacite (SiO_2 > 63 wt.%), and (3) monzonite gabbro (SiO_2 = 45–62 wt.%; Tables 1 and 2; Fig. 2a). The majority of samples have (Na_2O-2) < K_2O, which is typical of rocks with calc-alkaline affinities. Although most of the shoshonitic–latitic lavas are quartz-normative (up to 16% Q), many of them have olivine or nepheline in the norm; the same characteristics are observed in samples of the plutonic bodies. Likewise, dacites occurring both as extrusive ignimbrites and as shallowly intrusive domes are Q-normative (19.70%–30.05%).

4.2. Variation diagrams

Variations in major and trace elements against SiO_2 are plotted in Fig. 2. With increasing SiO_2, concentrations of CaO, $Fe_2O_3^T$, MgO, MnO,

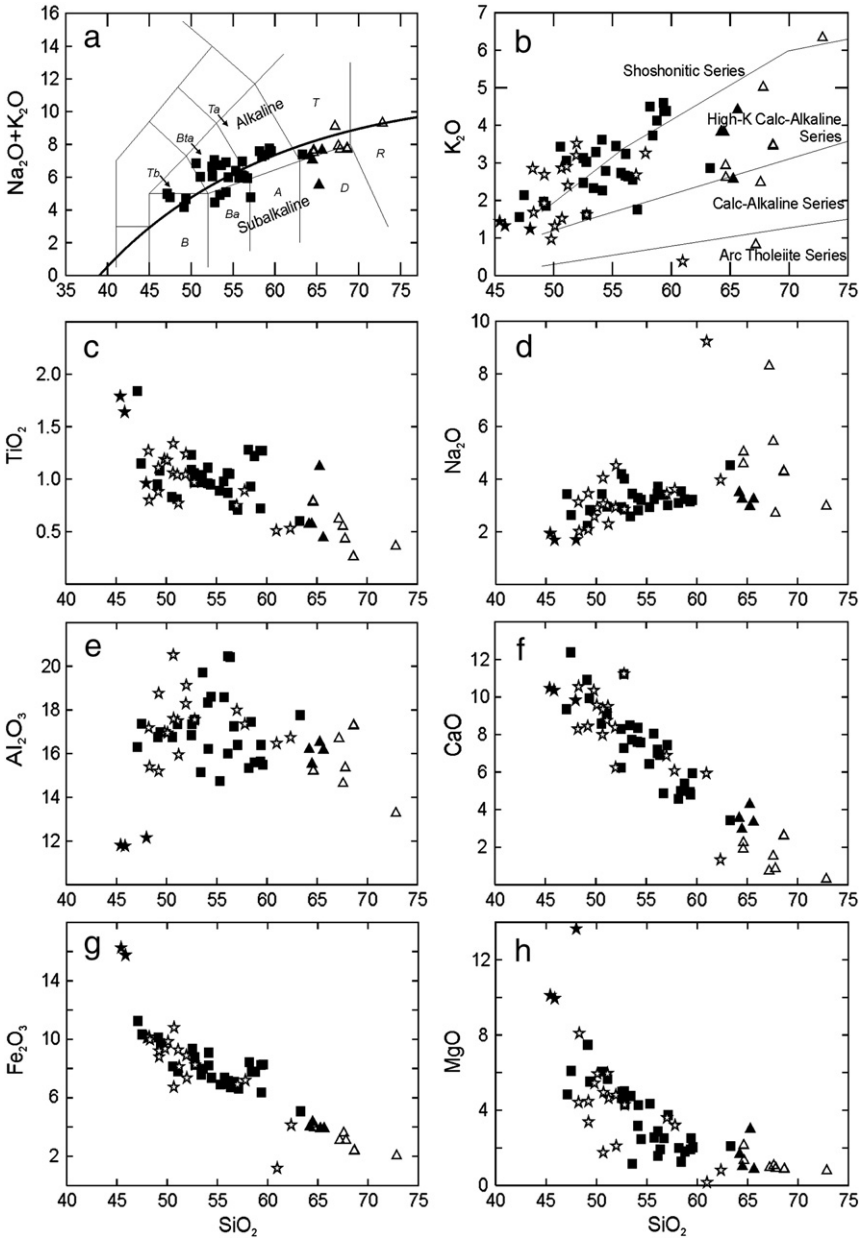

Fig. 2. Harker diagrams for volcanic rocks of the western AMA. Symbols used are as follows: basic–intermediate lavas = filled squares; dacitic ignimbrite = filled triangles; dacitic dome = open triangles; intrusive (sub-volcanic) bodies = open stars; cumulate intrusive bodies = filled stars.

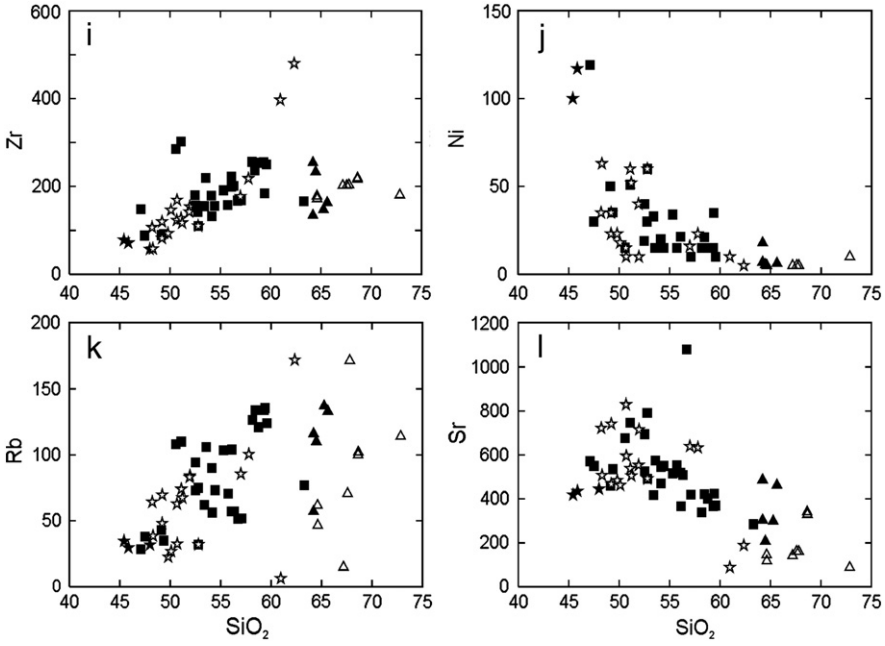

Fig. 2 (*continued*)

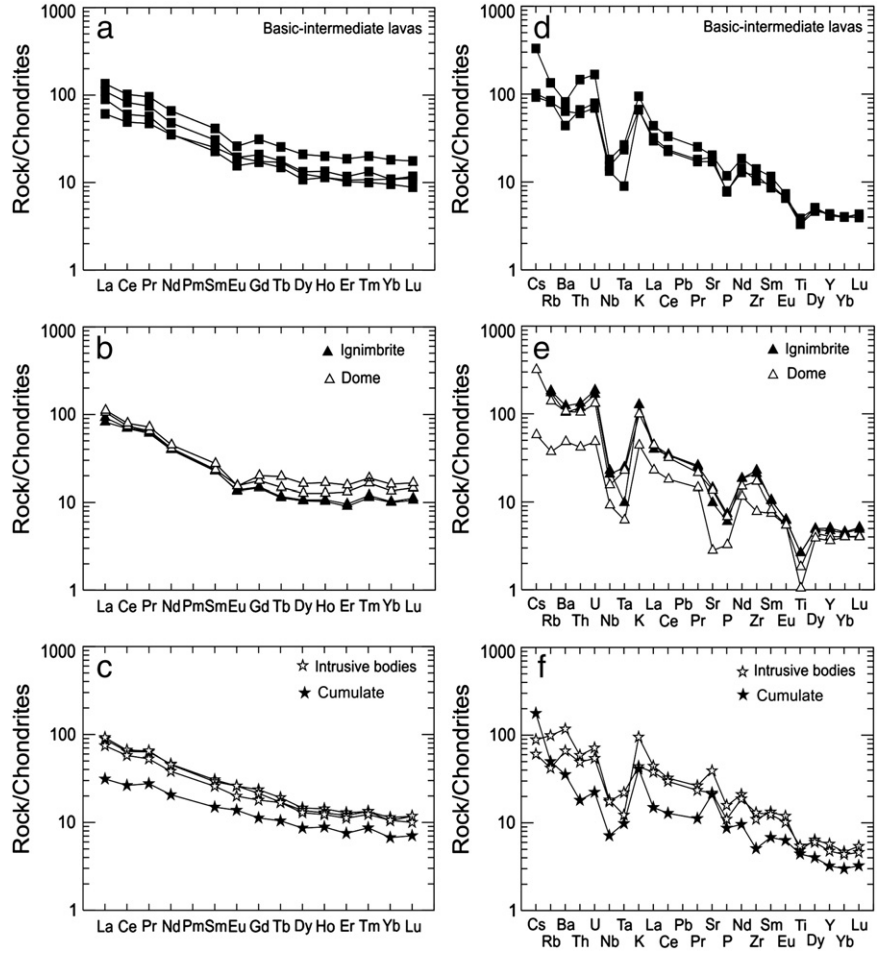

Fig. 3. a–c) Chondrite-normalized (Nakamura, 1974) and d–f) primitive mantle-normalized (Sun and McDonough, 1989) spider diagrams of volcanic and plutonic samples from the AMA. Symbols used are as follows: basic–intermediate lavas = filled squares; dacitic ignimbrite = filled triangles; dacitic dome = open triangles; intrusive (sub-volcanic) bodies = open stars; cumulate intrusive bodies = filled stars.

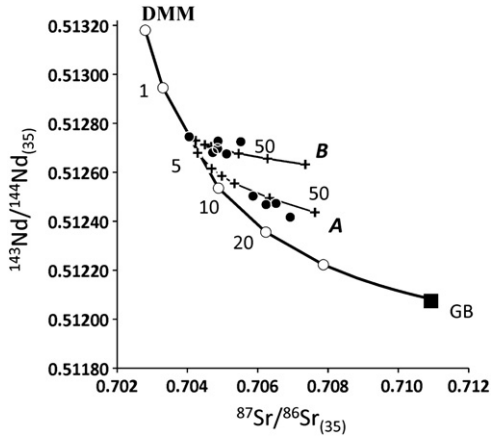

Fig. 4. $^{143}Nd/^{144}Nd$ and $^{87}Sr/^{86}Sr$ isotope variation diagram for Alborz magmatic rocks. The numbers along lines specify the percentage of added crustal sources (GB, A, B) to either DMM of one of the most basic samples (no. BA-1 in Table 1). Open circles: the percentages of granitic basement of Arabian Shield terrane (Sample No. 184417 in Stoeser and Frost, 2006) that was added to either a depleted or pristine mantle source (see Workman and Hart, 2005). Filled circles: the AMA samples. Abbreviations: DMM = Depleted MORB Mantle (Workman and Hart, 2005); GB = Granitic Basement (Stoeser and Frost, 2006); A, B = the proposed crustal sources.

Cr, Sc, Ni, and V decrease, whereas Na_2O, K_2O, Rb, Y, and Nb concentrations increase. Concentrations of Al_2O_3, TiO_2, P_2O_5, and Sr show a slight decrease with increasing SiO_2. Three samples from plutonic bodies show higher values than other plutonic samples in Al_2O_3, $Fe_2O_3^T$, MgO and TiO_2 vs. SiO_2 space. Based on this observation, we propose that these samples represent cumulates in the magma chamber.

4.3. Trace element variation

The analyzed samples were plotted in primitive mantle-normalized (Sun and McDonough, 1989) and rare earth element (REE)-normalized (Nakamura, 1974) spider diagrams (Fig. 3). All the rocks of the suite are characterized by REE patterns (Fig. 4a–c) which are flat for the MREE–HREEs, (~10× chondritic) and somewhat fractionated for the MREE – LREE, with LREE enriched to ~100 times chondrites. The flat MREE–HREE patterns clearly discount the role of garnet in the genesis of these samples. Both the felsic and mafic samples have very similar REE concentrations. The felsic rocks do however show moderate negative Eu-anomalies, though even the basaltic rocks have weak negative Eu-anomalies.

The extended trace element plots (Fig. 4d–f) show that the entire suite has strong negative Nb- and Ta-anomalies. This coupled with their enriched LILE values clearly implies subduction affiliation. Compared with the basalts, the felsic rocks have significant negative Sr-, P- and Ti-anomalies, implicating the potential roles for feldspar, apatite and Fe–Ti oxide fractionation.

4.4. Isotope geochemistry

Representative samples of the main rock types were analyzed for Sr, Nd, and Sm isotopes. The results are shown in Table 3, and initial ratios are plotted in Fig. 4.

Magmatic rocks of the AMA display the following range in Sr and Nd initial isotope ratios: $^{87}Sr/^{86}Sr_i = 0.704049–0.706925$ and $^{143}Nd/^{144}Nd_i = 0.512417–0.512745$ ($\varepsilon_{Nd(35)}$ +2.97 to −3.44). As shown in Fig. 4, the AMA magmas show isotopic signature of depleted MORB mantle (DMM) contaminated by a crustal sources (GB). Sr and Nd isotope ratios are negatively correlated though they tend to cluster in two groups or supposed trends (A and B in Fig. 4). It seems the AMA magmas were contaminated by the lower crustal sources (Fig. 5d) while they were differentiating (AFC process).

5. Discussion

The E–W-trending Alborz zone in northern Iran is a Cenozoic magmatic province. Volcanism in the zone was initiated in central Alborz during the Barremian, when alkaline olivine basalts were erupted (Wensink and Varekamp, 1980), and in the late Cretaceous with alkaline and tholeiitic rocks in the western Alborz zone (Salavati, 2008). However, the main volcanic event occurred in the early Eocene, beginning with explosive eruptions in a subsiding volcano-sedimentary basin (e.g., Annells et al., 1975; Dedual, 1967; Guest et al., 2006; Stöcklin and Eftekhar-Nezhad, 1969), then continuing with sub-aerial lava flows. The combination of extensional tectonism, arc magmatism, submarine deposition, rapid accumulation, and indicators of slumping and soft sediment deformation have been interpreted as reflecting sedimentation in a rapidly subsiding back-arc extensional basin related to rollback of the Neo-Tethys slab (e.g., Allen et al., 2003; Ballato et al., 2010; Brunet et al., 2003; Guest et al., 2006; Vincent et al., 2005).

Asiabanha (2006) subdivided the Eocene volcanic pile in the AMA (Karaj Formation) into two stages: shallow subaqueous volcaniclastic deposits (mostly in central Alborz) followed by sub-aerial lava flows (mostly in the western Alborz). The volcaniclastic deposits (or green tuffs) consist of both pyroclastic and epiclastic types and exhibit sedimentary structures. In contrast, the second stage of Eocene volcanism is characterized by various sub-aerial basic–acidic lava flows, including trachybasalt, trachyandesite, dacite, and rhyolite. The Eocene volcanic event in the AMA was then terminated by the intrusion of co-magmatic sub-volcanic bodies.

In the central Alborz, the Karaj Formation is underlain by evaporates of the Kond Formation (Davoudzadeh et al., 1997). These formations are in turn unconformably overlain by terrestrial clastic and evaporite deposits of the Oligocene lower Red Formation (e.g., Amini, 1997), which may have been associated with a regional

Table 3
Whole-rock Sm–Nd and Rb–Sr isotopic compositions of the Alborz magmatic assemblage, northern Iran.

Sample	$^{147}Sm/^{144}Nd$	$^{143}Nd/^{144}Nd$ (T = 0)	$^{143}Nd/^{144}Nd$ (T = 35)	2σ	ε_{Nd} (T = 35)	$^{87}Sr/^{86}Sr$ (T = 0)	$^{87}Sr/^{86}Sr$ (T = 35)	$^{87}Rb/^{86}Sr$	2σ
AL-1	0.1187	0.512500	0.512473	0.0000085	−2.35	0.706911	0.706521	0.784	0.000017
AM-4	0.0067	0.512729	0.512727	0.0000125	2.62	0.705082	0.704870	0.427	0.000011
AM-10	0.0728	0.512713	0.512696	0.0000094	2.02	0.705085	0.704856	0.462	0.000014
Zar-2	0.1255	0.512754	0.512725	0.0000088	2.57	0.705709	0.705518	0.385	0.000013
SZ-3	0.1237	0.512773	0.512745	0.0000085	2.97	0.704508	0.704049	0.924	0.000011
B-10	0.1144	0.512443	0.512417	0.0000086	−3.44	0.706994	0.706925	0.138	0.000012
A-131	0.1894	0.512724	0.512681	0.0000086	1.71	0.705381	0.704720	1.33	0.000013
SOL-1	0.1077	0.512493	0.512468	0.0000086	−2.44	0.706684	0.706238	0.897	0.000014
GAR-2	0.1318	0.512705	0.512675	0.0000114	1.60	0.705207	0.705114	0.188	0.000014
B14-6	0.1167	0.512529	0.512503	0.0000087	−1.76	0.706096	0.705867	0.459	0.000017

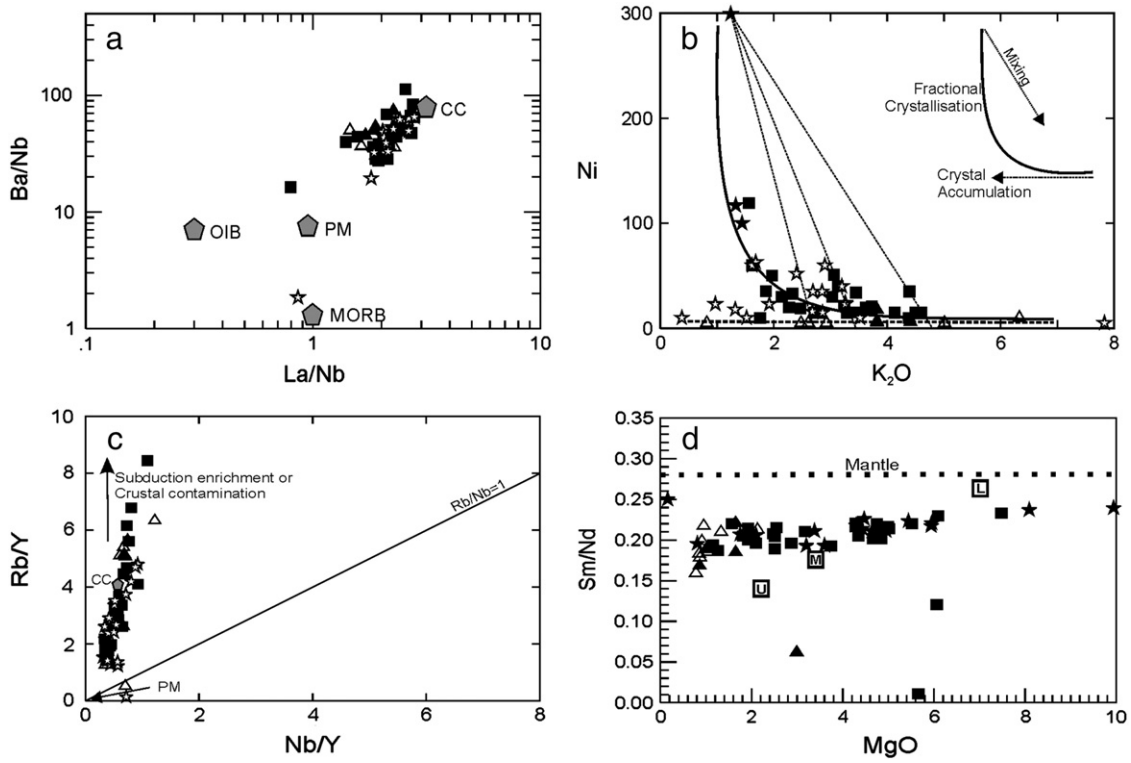

Fig. 5. Plots of trace element ratios showing: a) Ba/Nb vs. La/Nb (PM = primary mantle; OIB = ocean island basalt; MORB = mid-ocean ridge basalt; CC = continental crust) (data of PM, OIB, and MORB are from Sun and McDonough (1989), whereas CC data are from Rudnick and Gao (2003)); b) Ni vs. K_2O, which is useful for discriminating between fractional crystallization and mixing trends. Note that the cumulate samples form a horizontal array; c) Rb/Y vs. Nb/Y plot, showing the roles of subduction, enrichment, and crustal contamination in the evolution of the magmas (data of CC from Rudnick and Gao (2003)); d) MgO vs. Sm/Nd (from Nicholson et al., 2010) indicating varying levels of crustal assimilation and/or partial melting within AMA samples (U, M and L are upper, middle and lower crustal sources respectively). Symbols are as follows: basic–intermediate lavas = filled squares; dacitic ignimbrite = filled triangles; dacitic dome = open triangles; intrusive (sub-volcanic) bodies = open stars; cumulate intrusive bodies = filled stars.

phase of shortening during the late Eocene–early Oligocene (e.g., Berberian and King, 1981).

5.1. Processes contributing to petrological evolution

Because of some strong inverse correlations in some Harker diagrams (Fig. 2) (such as MgO, $Fe_2O_3^T$, CaO, TiO_2 and Ni against SiO_2), it seems that they indicate a genetic relationship. However, such a conclusion is not verified strictly by another plot (e.g., Al_2O_3 and P_2O_5 against SiO_2).

To simulate the conditions governing the evolution of magma in the chamber, the PELE program (Boudreau, 1999) was used. One of the most basic samples (Sample no. BA-1 in Table 1) was selected as the parental magma, and variations in a range of parameters (temperature and pressure, oxygen fugacity, and different phases involved in fractionation) were tested. Based on these tests, the optimum situation for producing such derivative liquids coincides with a temperature range of 700–1097 °C, at shallow depth ($P \approx 700$ bar).

Regardless of this inference, the trends observed in Harker plots could be explained by the fractionation of ol + cpx + Fe–Ti oxides in the basic to intermediate samples, and plg + bio ± hbl in intermediate to acidic rocks.

However, the role of crustal contamination in the evolution of magma compositions is verified by trace element and isotopic compositions (Fig. 5). Moreover, as shown in Fig. 5a,d, most samples fall between primitive mantle and continental crust, and additional evidence of crustal contamination is evident in Fig. 5b, c. Although the majority of data in Fig. 5b plot along a fractional crystallization trend, some fall on straight mixing lines.

5.2. AFC modeling

AFC modeling was based on the calculations of DePaolo (1981) and Aitcheson and Forrest (1994), using a composition for DMM from Workman and Hart (2005). Appropriate Sr–Nd isotopic data from either the continental crust of Iran or its basement are unavailable. Thus, because of the similarity of the Iranian basement to the Arabian–Nubian platform in the Precambrian, in particular their shared Gondwanan affinities and similar chemical compositions (granitic; Brunet et al., 2003; Hassanzadeh et al., 2008), a 600 Ma (Stoeser and Frost, 2006) granitic pluton from the Arabian platform (J Za'abah Pluton was used for the purpose of mixing calculations.

Fig. 4 shows isotopic data for volcanic rocks of the Alborz zone. The samples plot in two groups within the mantle array, one group with $^{143}Nd/^{144}Nd > 0.5126$, and the other with $^{143}Nd/^{144}Nd < 0.5125$, together with a higher radiogenic Sr content. The high ε_{Nd} samples tend to have relatively unradiogenic Sr isotopes. These data indicate that the AMA magmas were derived from a mantle source and were then modified by the crustal components.

Fig. 6 shows the results of calculations for determining the fraction of magma remaining in the chamber (F), based on a 40% mixture between the two sources of magma in the AMA ($r = 0.4$). Moreover, according to Figs. 4 and 6c, the samples of AMA have been grouped in two evolutionary trends that were controlled by AFC (high assimilation rate) and fractional crystallization processes.

5.3. Tectonic setting of the AMA

The Eocene volcanic and plutonic rocks of the AMA show clear evidence of their formation in subduction zone and collisional environments (Figs. 3, 5c, 7a–c). The most important geochemical

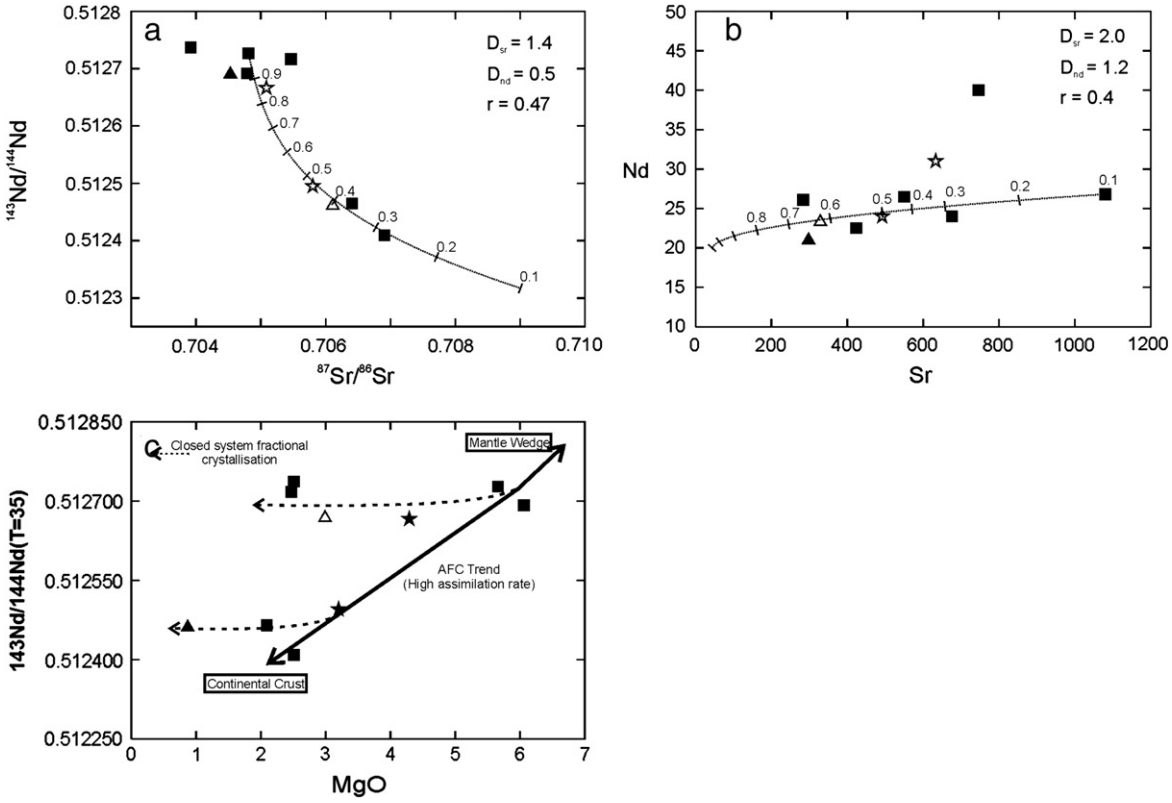

Fig. 6. a,b) Assimilation and fractional crystallization calculations (DePaolo, 1981) illustrating the effects of crustal contamination. The ratio of assimilation to fractional crystallization was assumed to be 0.4 (r = 0.4) in both plots. The numbers on the lines specify the parameter F (fraction of melt remaining in the chamber during crystallization). c) The arrangement of AMA samples in two proposed trends of fractional crystallization separated from AFC trend with high assimilation rate (Also note to Fig. 4). Symbols used are as follows: basic–intermediate lavas = filled squares; dacitic ignimbrite = filled triangles; dacitic dome = open triangles; intrusive (sub-volcanic) bodies = open stars; cumulate intrusive bodies = filled stars.

evidence for such processes is as follows: high-K calc-alkaline affinity of the magmatic series (Fig. 2b); enrichment in LREEs and LILEs (especially K, U, and Sr); depletion in some HFSEs (especially Nb, Ta, Ti, and Zr); high Th/Ta and Rb/Nb ratios; and negative anomalies in Ba and Ce (Fig. 3). However, the depletion of HFSEs and $^{143}Nd/^{144}Nd > 0.5126$ in some samples (Fig. 4) can also be explained by a high degree of partial melting of more depleted mantle material (Leeman et al., 2005; Rowe et al., 2009) and high water content in the source region (Stolper and Newman, 1994). Nevertheless, higher $^{87}Sr/^{86}Sr$ ratios in other samples, negative anomalies in Ba and Ce, and AFC modeling (Fig. 4) confirm that the mantle source magmas were significantly contaminated by a crustal component (Bacon, 1990; Kuscu and Geneli, 2010). Such components may be upper continental crust, underplated slab material, or even freshly subducted sediments. According to Avanzinelli et al. (2008), the depletion of Ba in volcanic rocks may be independent of the degree of silica saturation, and may instead reflect the composition of the sedimentary rocks from which the magmatic rocks were derived.

Although the association of the AMA with Neotethyan subduction and the subsequent collision of the Arabian and Eurasian lithospheres is widely accepted, the relatively large distance (200–500 km) between the AMA and the Neotethyan suture (Zagros thrust), together with the existence of two simultaneously juxtaposed volcanic arcs (AMA and UDMA), make a clear tectonic interpretation difficult.

To determine the role of subduction-related petrogenetic processes in the UDMA and AMA, the ratio vs. ratio trace element plots of Condie (2005) (Fig. 7d) and of Pearce and Stern (2006) (Fig. 7e) were used. For this purpose, data for the AMA (from this study) were compared with representative data for the UDMA from Mobarhan and Ahmadipour (2010) and Omrani et al. (2008) (Fig. 7e). The plot of Th/Ta (as a proxy for a deep subduction component) against Nb/Ta (a proxy for mantle depletion and degree of melting; Fig. 7e) shows that variability in the degree of partial melting of the mantle is higher in the AMA than in the UDMA. However, Pearce et al. (2005) stated that Nb/Ta ratios of more than 20 are related to lithospheric components that are mobilized during the rifting process. Thus, it can be concluded that both subduction and rifting processes contributed to the AMA.

Alavi (2007) and Sosson et al. (2010) proposed northern and southern branches for the Neotethys Ocean, with separate subduction zones for each. It has been suggested that the Tabriz–Takestan Fault is an Iranian suture of the northern Neotethys (Alavi, 2007), and the Izmir–Ankara–Erzincan–Sevan suture has been proposed for the northern Neotethys in Turkey (Sosson et al., 2010). However, there is no reliable stratigraphic or geochemical evidence for the existence of two separate Neotethyan oceans in Iran.

In contrast, Brunet et al. (2003) suggested that the Achara–Trialet, Ervan–Ordubad, Talesh, and southern Alborz Eocene basins began evolving in response to Cretaceous rifting, before undergoing a compressional regime at the end of the Cretaceous–Paleocene during closure of the back-arc domain of the Neotethys subduction zone. As evidence for this scenario, Brunet et al. (2003) cite the development of deep narrow basins (often under marine conditions) and calc-alkaline volcanism, trending towards alkaline. The accompaniment of Eocene volcanic eruptions by regional extension was also suggested by Vincent et al. (2005), Verdel (2008), and Ballato et al. (2010). According to these authors, the extensional tectonism, arc magmatism, submarine deposition, rapid accumulation, and indicators of slumping and soft sediment deformation can all be interpreted as reflecting sedimentation in a rapidly subsiding back-arc extensional basin during rollback of the Neotethys slab.

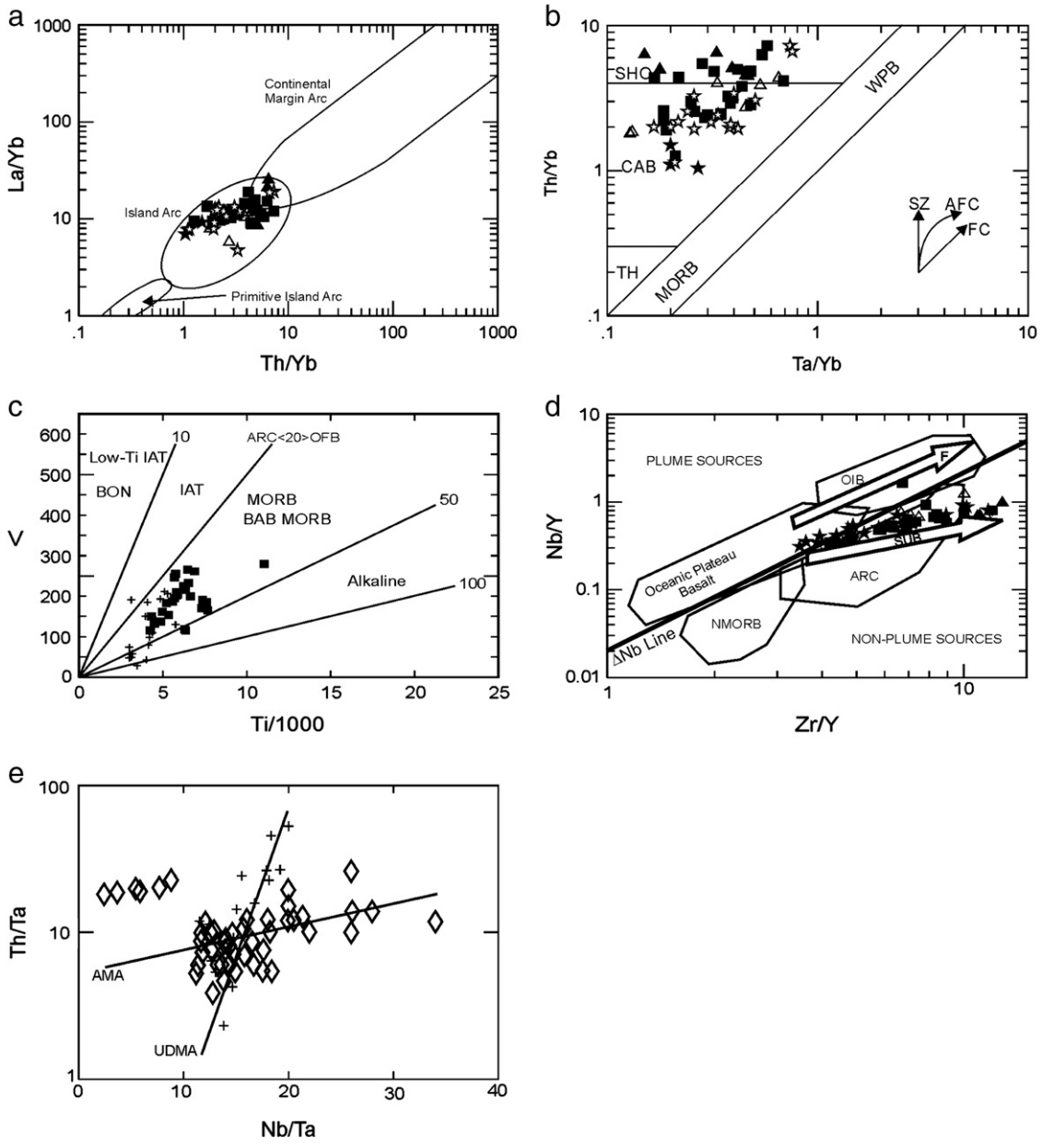

Fig. 7. Tectonic discrimination diagrams for volcanic rocks of the AMA: a) La/Yb vs. Th/Yb diagram (after Condie, 1989); b) Th/Yb vs. Ta/Yb diagram (after Pearce, 1983) Vectors show trends produced by addition of subduction zone (SZ) components, assimilation–fractional crystallization (AFC), and fractional crystallization (FC). c) V vs. Ti diagram (Shervais, 1982) [AB = Alkali Basalts; BAB = Back-arc Basalts; CB = Calc-alkaline Basalts; CFB = Continental Flood Basalts; IAT = Island Arc Tholeiites; MORB = Mid-ocean Ridge Basalts; OIB = Ocean Island Basalts]; d) Zr/Y vs. Nb/Y (Condie, 2005) showing fields for basalts from various tectonic settings. Arrows indicate effects of batch melting (F) and subduction (SUB). (ARC = Arc-related basalts; NMORB = Normal ocean ridge basalts; OIB = Ocean island basalts); e) plot of Th/Ta (as a proxy for a deeply subducted source component) vs. Nb/Ta (a proxy for mantle depletion and degree of partial melting; after Pearce and Stern, 2006) for volcanic rocks of the AMA and UDMA; Symbols are as follows: basic–intermediate lavas = filled squares; dacitic ignimbrite = filled triangles; dacitic dome = open triangles; intrusive (sub-volcanic) bodies = open stars; cumulate intrusive bodies = filled stars; volcanic rocks of UDMA = crosses; volcanic rocks of AMA = diamond.

Finally, geophysical studies have revealed two interesting characteristics of the Alborz zone. (1) Whereas crustal roots are well developed for other mountain belts within the broad Arabia–Eurasia collision (e.g., the Zagros Mountains), the Moho beneath the Alborz appears to be flat, and the thickness of the crust (~35 km) is similar to that of adjacent basins (Tatar, 2001). (2) Tomographic studies of the upper mantle in the Middle East have revealed extensive regions with positive velocity anomalies, at depths of up to 2200 km (Van der Voo et al., 1999). It has been inferred that these anomalies represent subducted Neotethys oceanic lithosphere beneath central and southern Iran. In addition, local tomographic studies in Iran indicate that these inferred slab relicts are only partially connected to the Arabian plate along the Zagros Mountains (Alinaghi et al., 2007), suggesting that the Neotethys slab was partially detached during continental collision (Paul et al., 2010).

Based on a combination of the above evidence, we propose the following model of volcanism in the Alborz zone in relation to the subduction of Neotethys and the closure of Arabia and Eurasia (Fig. 8):

1) *Formation of back-arc embryonic oceanic lithosphere* (Fig. 8a): According to Brunet et al. (2003), rift basins were formed during the Cretaceous in both southern Alborz and areas to the west (Achara-Trialet, Ervan-Ordubad, and Talesh). Moreover, Salavati (2008) reported an ophiolitic sequence in the western Alborz from the upper Cretaceous, suggesting that the ophiolite, which has a tholeiitic affinity, was formed in a back-arc setting. Thus,

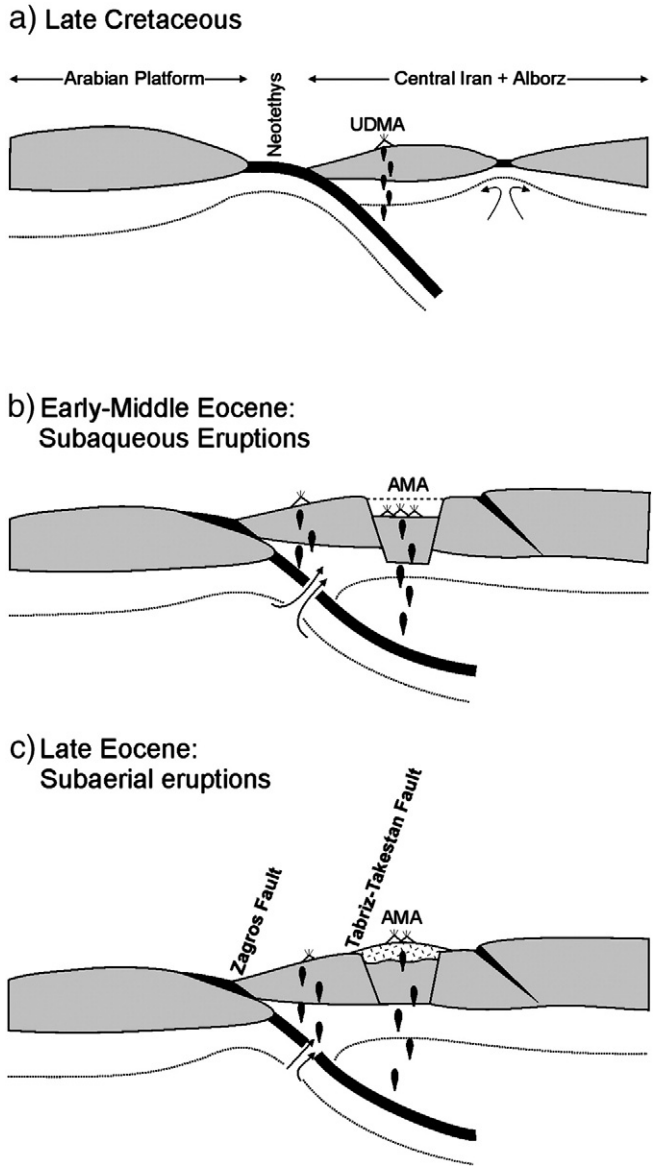

Fig. 8. Schematic illustration of the tectono-magmatic evolution of the Alborz magmatic assemblage: a) subduction of the Neotethys and formation of oceanic rift basins (late Cretaceous); b) formation of back-arc narrow marine basins, with clastic sedimentation and explosive eruptions (early–middle Eocene); and c) shoshonitic sub-aerial volcanism after uplift of the Alborz (upper Eocene).

we propose that an embryonic oceanic lithosphere originated behind the Neotethys suture and was subsequently transformed into shallow-depth marine basins under a compressional regime during the end of the Cretaceous and into the Paleocene (Brunet et al., 2003).

2) *Back-arc narrow, shallow-depth basins* (Fig. 8b): After collision of Arabia and Eurasia in the Eocene (e.g., Allen et al., 2003; Beydoun et al., 1992; Dargahi et al., 2010; Ghasemi and Talbot, 2006; Hempton, 1987; Hessami et al., 2001), narrow shallow-depth marine basins were formed in southern Alborz; they were created along normal faults in a tensional crustal setting. After basin formation, explosive eruptions created volcaniclastic deposits. The southern volcano-sedimentary basin was removed at ca. 36 Ma (Ballato et al., 2010) by erosion during a compressional regime, and as a consequence the evaporitic and clastic sediments of the Kond and Upper Red formations were deposited unconformably over the Karaj Formation.

3) *Shoshonitic sub-aerial volcanism* (Fig. 8c): After the removal by erosion of the volcano-sedimentary basin in central Alborz, sub-aerial volcanic eruptions of considerable volume occurred in western Alborz (e.g., Asiabanha, 2001; Ebrahimi, 2000). These volcanic rocks belong to the potassic calc-alkaline suite, and their geochemical signatures indicate a mantle source that was variably contaminated by crustal components. Moreover, they have features reflecting genesis in a continental collision environment.

6. Conclusions

Eocene volcanism in the AMA has a complex tectono-magmatic history, and involved explosive eruptions in narrow, shallow-depth marine basins, followed by sub-aerial effusive eruptions. The stratigraphic and structural study by Allen et al. (2003) shows that volcaniclastic deposits of the AMA were formed during an extensional phase in the early Eocene and we propose them as the back-arc extensional basins. However, because of basin uplift during a compressional regime in the late Eocene, the later volcanic phase (effusive eruptions) occurred sub-aerially, and farther to the west.

The volcanic and sub-volcanic rocks of the AMA belong to the high-K calc-alkaline (or shoshonitic) suite, and are associated with continental collision settings. Their enrichment in LREEs and LILEs (especially K, U, and Sr), and depletion in some HFSEs (Nb, Ta, Ti, and Zr), is consistent with a subduction environment.

Variation diagrams verify that their magmatic evolution was dominated by fractional crystallization at shallow levels in the lithosphere. However, crystallization modeling using the PELE program reveals that the magma system was open to some chemical exchange, in particular for Al_2O_3 and SiO_2. This conclusion is further supported by isotopic and trace element evidence. Thus, we propose that an AFC mechanism was responsible for magmatic evolution in the AMA.

Differences in isotopic compositions (rocks form two distinct clusters: one with $\varepsilon_{Nd} > 0$, the other with $\varepsilon_{Nd} < 0$ and higher Sr isotope ratios) confirm that the magmas were derived from a depleted mantle source that was later contaminated by crustal materials during ascent through the continental lithosphere. Moreover, comparisons between the AMA and UDMA suggest that variability in degrees of partial melting and mantle enrichment was higher in the AMA than in the UDMA. Thus, it can be inferred that the source region of AMA magmas was influenced by various components, including deeply subducted lithosphere and partial melts of lithosphere in an extensional back-arc setting.

Acknowledgments

This study was performed as part of a collaborative research project (sabbatical) between IKIU and Adelaide University and supported by the IKIU Grant No. 751268–1391. Reviews by Kirsten Nicholson and Michael Roden, and editorial comments by Nelson Eby helped to improve greatly the manuscript. Special thanks dedicated to David Bruce for his assistance in the isotope laboratory of Adelaide University.

References

Agard, P., Omrani, J., Jolivet, L., Mouthereau, F., 2005. Convergence history across Zagros (Iran): constraints from collisional and earlier deformation. International Journal of Earth Sciences 94, 401–419. http://dx.doi.org/10.1007/s00531-005-0481-4.

Aitcheson, S.J., Forrest, A.H., 1994. Quantification of crustal contamination in open magmatic systems. Journal of Petrology 35, 461–488.

Alavi, M., 1996. Tectonostratigraphic synthesis and structural style of the Alborz Mountain system in Northern Iran. Journal of Geodynamics 21, 1–33.

Alavi, M., 2004. Regional stratigraphy of the Zagros fold-thrust belt of Iran and its proforeland evolution. American Journal of Science 304, 1–20.

Alavi, M., 2007. Structures of the Zagros fold-thrust belt in Iran. American Journal of Science 307, 1064–1095.

Alinaghi, A., Koulakov, I., Thybo, H., 2007. Seismic tomographic image of P-and S-waves velocity perturbations in the upper mantle beneath Iran. Geophysical Journal International 169, 1089–1102. http://dx.doi.org/10.1111/j.1365-246X.2007.03317.x.
Allen, M.B., Ghassemi, M.R., Shahrabi, M., Qorashi, M., 2003. Accommodation of late Cenozoic oblique shortening in the Alborz range, northern Iran. Journal of Structural Geology 25, 659–672.
Amini, A., 1997. Provenance and Depositional Environment of Upper Red Formation, Central Zone, Iran. Unpublished Ph.D. Thesis, University of Manchester, Manchester, 320 pp.
Annells, R.N., Arthurton, R.S., Bazely, R.A., Davis, R.G., 1975. Explanatory text of the Qazvin and Rasht quadrangles map (1:250000). Geological Survey of Iran.
Asiabanha, A., 2001. Geology and Petrogenesis of Volcanic Facies In Youzbashi-Chai, W-Qazvin. Unpublished Ph.D. Thesis, Tarbiat Modarres University, IR Iran, 321 pp.
Asiabanha, A., 2006. A Paleogene two-stage volcanism in the Alborz zone, Iran. Proceedings of International Conference on Continental Volcanism, Guangzhou, China.
Asiabanha, A., Ghasemi, H., Meshkin, M., 2009. Paleogene continental-arc type volcanism in North Qazvin, North Iran: facies analysis and geochemistry. Neues Jahrbuch für Mineralogie Abhandlungen 186, 201–214.
Avanzinelli, R., Elliot, T., Tommasini, S., Conticeli, S., 2008. Constraints on the genesis of potassium-rich Italian volcanic rocks from U/Th disequilibrium. Journal of Petrology 49, 195–223.
Axen, G.J., Lam, P.S., Grove, M., Stockli, D.F., 2001. Exhumation of the west-central Alborz Mountains, Iran, Caspian subsidence, and collision-related tectonics. Geology 29, 559–562.
Azizi, H., Moinevaziri, H., 2009. Review of the tectonic setting of Cretaceous to Quaternary volcanism in northwestern Iran. Journal of Geodynamics 47, 167–179.
Bacon, C.R., 1990. Calc-alkaline, shoshonitic, and primitive tholeiitic lavas from monogenetic volcanoes near Crater Lake, Oregon. Journal of Petrology 31, 135–166.
Ballato, P., Uba, C.E., Landgraf, A., Strecker, M.R., Sudo, M., Stockli, D.F., Friedrich, A., Tabatabaei, S.H., 2010. Arabia–Eurasia continental collision: insights from late Tertiary foreland-basin evolution in the Alborz Mountains, northern Iran. Geological Society of America Bulletin. http://dx.doi.org/10.1130/B30091.1.
Berberian, M., 1981. The south Caspian: a compressional depression floored by a trapped, modified oceanic crust. Canadian Journal of Earth Science 20, 163–183.
Berberian, M., 1983. Generalized tectonic Map of Iran. Geological Survey of Iran Report No. 52.
Berberian, M., King, G.C.P., 1981. Towards a paleogeography and tectonic evolution of Iran. Canadian Journal of Earth Sciences 18, 210–265. http://dx.doi.org/10.1139/e81-163.
Berberian, F., Muir, I.D., Pankhurst, R.J., Berberian, M., 1982. Late Cretaceous and early Miocene Andean type plutonic activity in northern Makran and central Iran. Journal of the Geological Society of London 139, 605–614.
Beydoun, Z.R., Hughes Clarke, M.W., Stoneley, R., 1992. A late Tertiary foreland basin overprinted onto the outer edge of a vast hydrocarbon-rich Paleozoic–Mesozoic passive-margin shelf. Foreland Basins and Fold Belts: In: Macqueen, R.W., Leckie, D.A. (Eds.), Petroleum in the Zagros Basin: American Association of Petroleum Geologist Memoir, 55, pp. 309–339.
Boudreau, A.E., 1999. PELE-a version of the MELTS software program for the PC platform. Computers and Geosciences 25, 201–203.
Brunet, M.F., Korotaev, M.V., Ershov, A.V., Nikishin, A.M., 2003. The South Caspian Basin: a review of its evolution from subsidence modelling. Sedimentary Geology 156, 119–148. http://dx.doi.org/10.1016/S0037-0738(02)00285-3.
Condie, K.C., 1989. Geochemical changes in basalts and andesites across the Archean–Proterozoic boundary: identification and significance. Lithos 23, 1–18.
Condie, K.C., 2005. High field strength element ratios in Archean basalts: a window to evolving sources of mantle plumes? Lithos 79, 491–504.
Dargahi, S., Arvin, M., Pan, Y., Babaei, A., 2010. Petrogenesis of post-collisional A-type granitoids from the Urumieh–Dokhtar magmatic assemblage, Southwestern Kerman, Iran: constraints on the Arabian–Eurasian continental collision. Lithos 115, 190–204.
Davoudzadeh, M., Lammerer, B., Weber-Diefenbach, K., 1997. Paleogeography, stratigraphy, and tectonics of the Tertiary of Iran. Neues Jahrbuch für Geologie und Palaontologie, Abhandlungen 205, 33–67.
Dedual, E., 1967. Zur Geologie Dest Mittleren Und Unteren Karaj-Tales, Zentral Elburz (Iran). Unpublished Ph.D. Thesis, University of Zurich, Zurich, 125 pp. (in German).
DePaolo, D.J., 1981. Trace element and isotopic effects of combined wall rock assimilation and fractional crystallization. Earth and Planetary Science Letters 53, 189–202.
Ebrahimi, M., 2000. A study on the petrology and mineralogy of the Mesozoic volcanic rocks of Pinggang-Veijing area in Northeastern China and the Paleogene volcanic rocks of Molla-Ali area in Northwestern Iran. Unpublished Ph.D. Thesis, China University of Geosciences, China, 101 pp.
Foden, J., Mawby, J., Kelly, S., Turner, S., Bruce, D., 1995. Metamorphic events in the eastern Arunta Inlier, Part 2. Nd–Sr–Ar isotopic constraints. Precambrian Research 71, 207–227.
Ghasemi, A., Talbot, C.J., 2006. A new scenario for the Sanandaj–Sirjan zone (Iran). Journal of Asian Earth Sciences 26, 683–693.
Guest, B., Axen, G.J., Lam, P.S., Hassanzadeh, J., 2006. Late Cenozoic shortening in the west-central Alborz Mountains, northern Iran, by combined conjugate strike-slip and thin-skinned deformation. Geosphere 2, 35–52. http://dx.doi.org/10.1130/GES00019.1.
Hassanzadeh, J., Ghazi, A.M., Axen, G., Guest, B., 2002. Oligomiocene mafic-alkaline magmatism north and northwest of Iran: evidence for the separation of the Alborz from the Urumieh–Dokhtar magmatic arc. Geological Society of America Abstracts with Programs 34, 331.
Hassanzadeh, J., Stockli, D.F., Horton, B.K., Axen, G.J., Stockli, L.D., Grove, M., Schmitt, A.K., Walker, J.D., 2008. U–Pb zircon geochronology of late Neoproterozoic–Early Cambrian granitoids in Iran: implications for paleogeography, magmatism, and exhumation history of Iranian basement. Tectonophysics 451, 71–96.
Hempton, M.R., 1987. Constraints on Arabian plate motion and extensional history of the Red Sea. Tectonics 6, 687–705.
Hessami, K., Koyi, H.A., Talbot, C.J., Tabasi, H., Shabanian, E., 2001. Progressive unconformities within an evolving foreland fold-thrust belt, Zagros Mountains. Journal of the Geological Society of London 158, 969–981.
Jackson, J., Priestley, K., Allen, M., Berberian, M., 2002. Active tectonics of the South Caspian Basin. Geophysical Journal International 148, 214–245. http://dx.doi.org/10.1046/j.1365-246X.2002.01588.x.
Kuscu, G.G., Geneli, F., 2010. Review of post-collisional volcanism in the Central Anatolian volcanic Province (Turkey), with special reference to the Tepekoy volcanic Complex. International Journal of Earth Sciences 99, 593–621.
Lasemi, Y., 1992. Submarine fans and turbidite deposits in the Karaj Formatin (Abstract). 10th Geosciencc Meeting of the Geological Survey of Iran, p. 5.
Leeman, W.P., Lewis, J., Evarts, R.C., Conrey, R.M., Streck, M.J., 2005. Petrologic constraints on the thermal structure of the Cascades arc. Journal of Volcanology and Geothermal Research 140, 67–105.
McCall, G.J.H., 1997. The geotectonic history of the Makran and adjacent areas of southern Iran. Journal of Asian Earth Sciences 15, 517–531.
Mobarhan, S.K., Ahmadipour, H., 2010. Using magma mixing/mingling evidence for understanding magmatic evolution at Mount Bidkhan Stratovolcano (South-East Iran). Journal of Sciences, Islamic Republic of Iran 21, 137–153.
Nakamura, N., 1974. Determination of REE, Ba, Fe, Mg, Na and K in carbonaceous and ordinary chondrites. Geochimica et Cosmochimica Acta 38, 757–775.
Nicholson, K.N., Khan, M., Mahmood, K., 2010. Geochemistry of the Chagai–Raskoh arc, Pakistan: complex arc dynamics spanning the Cretaceous to the Quaternary. Lithos 118, 338–348.
Omrani, J., Agard, P., Whitechurch, H., Benoit, M., Prouteau, G., Jolivet, L., 2008. Arc-magmatism and subduction history beneath the Zagros Mountains, Iran: a new report of adakites and geodynamic consequences. Lithos 106, 380–398.
Paul, A., Hatzfeld, D., Kaviani, A., Tatar, M., Pequegnat, C., 2010. Seismic imaging of the lithospheric structure of the Zagros mountain belt (Iran). Tectonic and stratigraphic evolution of the Zagros and Makran during the Meso-Cenozoic: In: Leturmy, P., Robin, C. (Eds.), Geological Society of London Special Publication, 330, pp. 5–18. http://dx.doi.org/10.1144/SP330.2.
Pearce, J.A., 1983. Role of the sub-continental lithosphere in magma genesis at active continental margins. In: Hawkesworth, C.J., Norry, M.J. (Eds.), Continental Basalts and Mantle Xenoliths. Shiva, Nantwic, pp. 230–249.
Pearce, J.A., Stern, R.J., 2006. Origin of back basin magmas: trace element and isotope perspectives. Back-arc Spreading Systems: Geological, Biological, Chemical and Physical Interactions: In: Christie, D.M., Fisher, C.R., Lee, S.M., Givens, S. (Eds.), Geophysical Monograph Series, 166. http://dx.doi.org/10.1029/166GM06.
Pearce, J.A., Stern, R.J., Bloomer, S.H., Fryer, P., 2005. Geological mapping of the Mariana arc-basin systems: implications for the nature and distribution of subduction components. Geochemistry, Geophysics, Geosystems 6 (2004GC00895).
Rowe, M.C., Kent, A.J.R., Nielsen, R.L., 2009. Subduction influence on oxygen fugacity and trace and volatile elements in basalts across the Cascades arc. Journal of Petrology 50, 61–91.
Rudnick, R.L., Gao, S., 2003. The composition of the continental crust. In: Rudnick, R.L. (Ed.), The Crust. Elsevier-Pergamon, Oxford, pp. 1–64.
Salavati, M., 2008. Petrology, geochemistry and mineral chemistry of extrusive alkali rocks of the southern Caspian Sea ophiolite, Northern Alborz, Iran: evidence of alkaline magmatism in Southern Eurasia. Journal of Applied Sciences 8, 2202–2216.
Shahabpour, J., 2005. Tectonic evolution of the orogenic belt in the region located between Kerman and Neyriz. Journal of Asian Earth Sciences 24, 405–417.
Shervais, J.W., 1982. Ti–V plots and the petrogenesis of modern and ophiolitic lavas. Earth and Planetary Science Letters 59, 101–118.
Sosson, M., Kaymakci, N., Stephenson, R., Bergerat, F., Starostenko, V., 2010. Sedimentary basin tectonics from the Black Sea and Caucasus to the Arabian Platform: introduction. Geological Society, London, Special Publications 340, 1–10. http://dx.doi.org/10.1144/SP340.1.
Stampfli, G.M., 2000. Tethyan oceans. Tectonics and magmatism in Turkey and the surrounding area: In: Bozkurt, E., Winchester, J.A., Piper, J.D.A. (Eds.), Geological Society, London, Special Publications, 173, pp. 1–23.
Stampfli, G.M., Marcoux, J., Baud, A., 1991. Tethyan margins in space and time. Palaeogeography, Palaeoclimatology, Palaeoecology 87, 373–409.
Stöcklin, J., 1974. Possible ancient continental margins in Iran. In: Burk, C.A., Drake, C.L. (Eds.), The Geology of Continental Margins. Springer-Verlag, Berlin, pp. 873–887.
Stöcklin, J., Eftekhar-Nezhad, J., 1969. Explanatory text of the Zanjan quadrangle map (1:250000). Geological Survey of Iran 61 pp.
Stoeser, D.B., Frost, C.D., 2006. Nd, Pb, Sr, and O isotopic characterization of Saudi Arabian Shield terranes. Chemical Geology 226, 163–188.
Stolper, E., Newman, S., 1994. The role of water in the petrogenesis of Mariana Trough magmas. Earth and Planetary Science Letters 121, 293–325.
Sun, S.S., McDonough, W.F., 1989. Chemical and isotopic systematic of oceanic basalts: implications for mantle composition and processes. Magmatism in the ocean basins: In: Saunders, A.D., Norry, M.J. (Eds.), Geological Society, London, Special Publications, 42, pp. 313–345.
Tatar, M., 2001. Etude Seismotectonique de deux zones de collision continentale: le Zagros Central et l'Alborz (Iran). Unpublished Ph.D. Thesis, University de Joseph Fourier, France. (in French).
Van der Voo, R., Spakman, W., Bijwaard, H., 1999. Tethyan subducted slabs under India. Earth and Planetary Science Letters 171, 7–20. http://dx.doi.org/10.1016/S0012-821X(99)00131-4.

Verdel, C.S., 2008. Cenozoic Geology of Iran: An Integrated Study of Extensional Tectonics and Related Volcanism. Unpublished Ph.D. Thesis, California Institute of Technology, Pasadena, 182 pp.
Vincent, S.J., Allen, M.B., Ismail-Zadeh, A.D., Flecker, R., Foland, K.A., Simmons, M.D., 2005. Insights from the Talysh of Azerbaijan into the Paleogene evolution of the south Caspian region. Geological Society of America Bulletin 117, 1513–1533. http://dx.doi.org/10.1130/B25690.1.
Vincent, S.J., Morton, A.C., Carter, A., Gibbs, S., Barabadze, T.G., 2007. Oligocene uplift of the western Greater Caucasus: an effect of initial Arabia–Eurasia collision. Terra Nova 19, 160–166. http://dx.doi.org/10.1111/j.1365-3121.2007.00731.x.
Wensink, H., Varekamp, J.C., 1980. Paleomagnetism of basalts from Alborz: Iran part of Asia in the Cretaceous. Tectonophysics 68, 113–129.
Workman, R.K., Hart, S.R., 2005. Major and trace element composition of the depleted MORB mantle (DMM). Earth and Planetary Science Letters 231, 53–72.
Zanchi, A., Berra, F., Mattei, M., Ghassemi, M., Sabouri, J., 2006. Inversion tectonics in central Alborz, Iran. Journal of Structural Geology 28, 2023–2037. http://dx.doi.org/10.1016/j.jsg.2006.06.020.